Electronic Supplementary Material

High-performance hydrogen evolution of $MoSe_2$-Mo_2C seamless heterojunction enabled by efficient charge transfer

Jing Li, Wenting Hong, Chuanyong Jian, Qian Cai, Xu He, and Wei Liu *

J. Li, W. Hong, C. Jian, Dr. Q. Cai, Dr. X. He, Prof. W. Liu

CAS Key Laboratory of Design and Assembly of Functional Nanostructures, Fujian Institute of Research on the Structure of Matter, Chinese Academy of Sciences, Fuzhou, 350002, China Fujian Provincial Key Laboratory of Nanomaterials, Fujian Institute of Research on the Structure of Matter, Chinese Academy of Sciences, Fuzhou, 350002, China

E-mail: liuw@fjirsm.ac.cn

W. Hong，C. Jian

University of Chinese Academy of Sciences, Beijing, 100049, China

Structural characterizations

X-ray diffraction (XRD) spectra are obtained to detect the phase of samples using the D8 ADVANCE diffractometer with Cu Kα radiation (λ = 1.5418 Å). The morphology of the as-grown catalysts is characterized by scanning electron microscopy (HITACHI UHR FE-SEM SU8010). Transmission electron microscopy (TEM), high-resolution TEM (HRTEM), selected-area electron diffraction (SAED) and energy-dispersive X-ray spectroscopy (EDS) mapping studies are carried out on a probe-corrected transmission electron microscope operating at 200 kV (FEI Titan F20 TEM). X-ray photoelectron spectroscopy (XPS) measurements are performed by a ESCALAB 250Xi system (Thermo Fisher), equipped with a 100 W Al Kα source on a spot size of 100 μm at a 45° incident angle. The binding energy scan ranges from 0 to 1200 eV with an interval step of 1 eV, and the spectra are calibrated to carbon line of 284.8 eV. The Faradaic efficiency tests of the catalyst are conducted on a gas chromatography (Shimadzu, GC-2010 Plus) to measure the quantity of experimental H_2 generated during the 30 min HER process.

DFT Calculations

DFT calculations are carried out based on the HRTEM and XRD results, (100) and (101) planes of Mo_2C, (001) and (100) surfaces of $MoSe_2$ are clearly observed. The above-mentioned lattice planes are employed to study the intermediate adsorption on active sites. As for the hybridized $Mo_2C/MoSe_2$, the lattice mismatch for $Mo_2C/MoSe_2$ interface is calculated according to the following formula [1,2]:

$$lattice mismatch = \frac{M \cdot d_{Mo_2C} - N \cdot d_{MoSe_2}}{N \cdot d_{MoSe_2}} \times 100\% \quad (1)$$

here d_{Mo2C} refers to the Mo_2C lattice distance in Mo_2C plane; d_{MoSe2} refers to the $MoSe_2$ lattice distance in $MoSe_2$ plane, M and N are the weighted factors for lattice match. Hence, the lattice mismatch between Mo_2C-(100) and $MoSe_2$-(100) is -7%, which is smaller than that between Mo_2C-(101) and $MoSe_2$-(100) (~ -18%). Also, the lattice mismatch between Mo_2C-(101) and $MoSe_2$-(001) is 6%, which is smaller than that between Mo_2C-(100) and $MoSe_2$-(001) (~ 20%). The larger lattice mismatch is the main contribution to the larger strain in the resulted films, therefore Mo_2C(100)/$MoSe_2$(100) and Mo_2C(101)/$MoSe_2$(001) hybridized structures are chosen in our calculation.

DFT calculations are implemented in AtomistixToolKit (ATK) 2017.2 [3] with local density approximation (LDA) [4] exchange correlations, together with a double ζ polarized basis set for expanding electronic density. We employ a 2 × 2 × 1 Monkhorst–Pack [5] k-point grid with the cutoff energy of 500 eV. The Pulay mixer algorithm [6] controls the self-consistent iterations with 0.0002 Ry tolerance and 100 maximum steps. The structures are optimized to a maximum force of 0.001 eV/Å and the maximum stress of 0.0001 eV/Å^3 with a limited memory Broyden-Fletcher-Goldfarb-Shanno (LBFGS) algorithm.[7] The differential binding energy is used to describe the stability of hydrogen, defined as

$$\Delta E_H = E(M + nH) - E(M + (n\text{-}1)H) - 1/2E(H_2) \quad (2)$$

where $E(M + nH)$ is the total energy for the M substrate and n hydrogen atoms adsorbed on the edge, $E(M + (n-1)H)$ is the total energy for (n-1) adsorbed hydrogen atoms, and $E(H_2)$ is the energy of a gas phase hydrogen molecule. The Gibbs free energy for hydrogen adsorption (ΔG_H) can be calculated as

$$\Delta G_H = \Delta E_H + \Delta ZPE - T\Delta S_H \quad (3)$$

where ΔZPE is the zero-point energy difference between the adsorbed state of the system and the gas phase state, ΔS_H is the entropy difference between the adsorbed state of the system and the gas phase standard state (300 K, 1 bar). The ΔG_H on the possible active sites that adsorb H atom are calculated on Mo and C for Mo_2C, Mo and Se for $MoSe_2$, and Mo, C and Se in the interface for the hybridized $Mo_2C/MoSe_2$ composite. With DFT we also simulate the electrostatic features of electron difference density (EDD) for the $Mo_2C/MoSe_2$ junction to explore the charge transfer in the interface between those two materials.

The infinite, non-periodic $Mo_2C/MoSe_2$ interface relies on a two-probe setup in which a left (L) and a right (R) semi-infinite electron reservoirs are connected through a central (C) region containing the interface, as shown in Figure S1. In this way, we try to achieve a moderate band gap offset between the two materials. The chemical potentials μ_L and μ_R for the left and right electrodes have been defined, respectively, to obtain the electronic density in the C region. The projected local density of states (PLDOS) of the $Mo_2C/MoSe_2$ junction is plotted in Fig. 5d at μ_L-μ_R = - 0.25 V with the 13×13 k-point sampling. The chemical potential of the left electrode is higher in energy than that of right electrode. Consequently, there will be a net flow of electrons from the left to the right electrodes, the electrons have to overcome a potential barrier at interface due to the presence of the depletion region in $MoSe_2$.

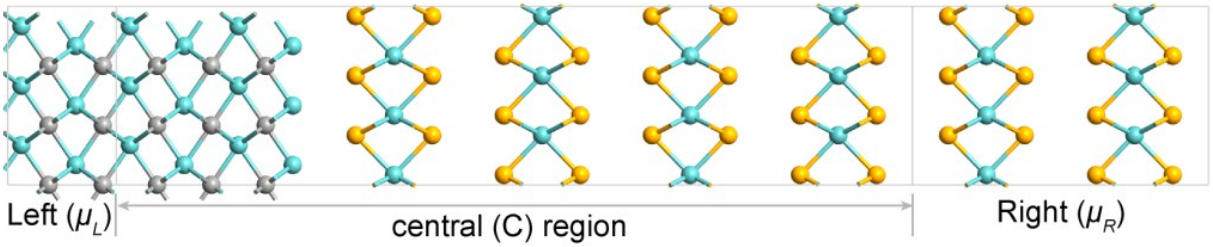

Fig. S1. Geometries employed to simulate the $Mo_2C/MoSe_2$ interface. The blue, gray, and yellow spheres represent Mo, C and Se atoms, respectively.

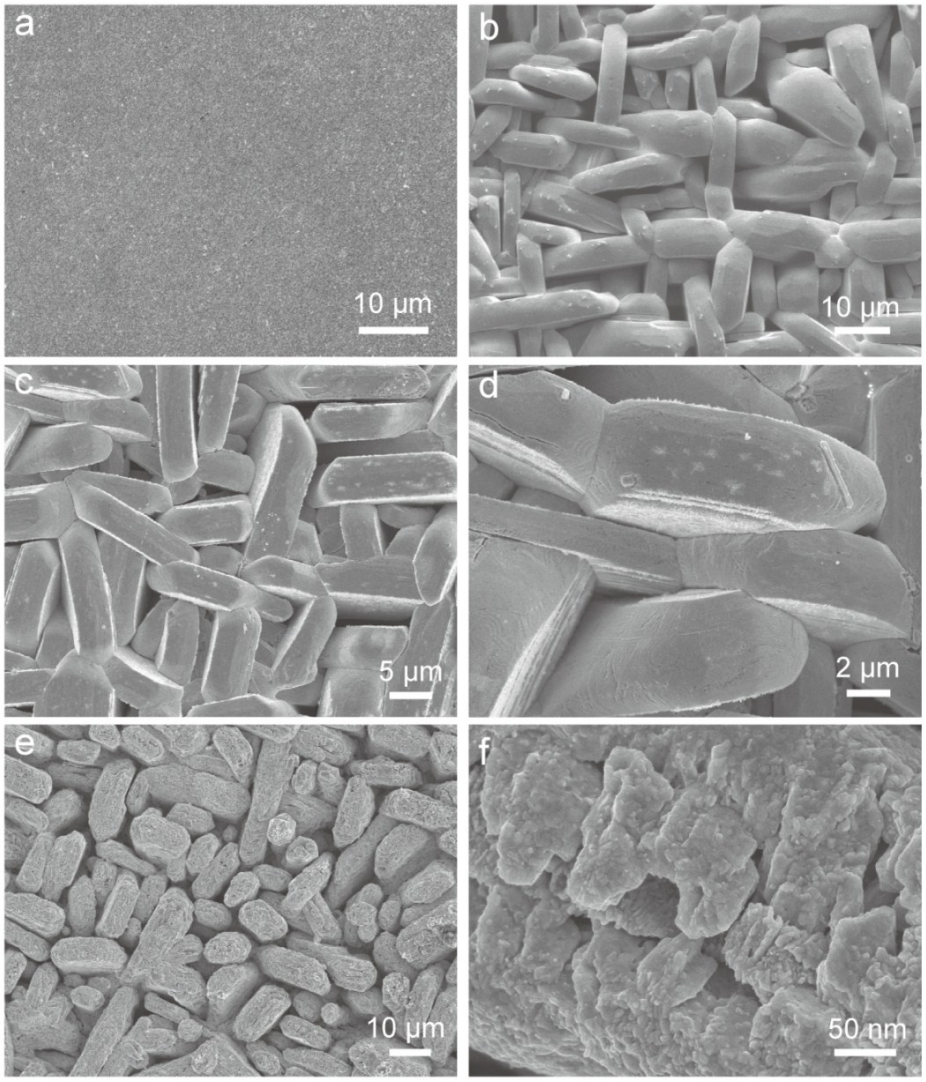

Fig. S2. SEM images of (a) prinstine Mo foil, (b) MoO_3 films, (c, d) Mo_2C with different magnifications, and (e, f) $Mo_2C/MoSe_2$ with different magnifications.

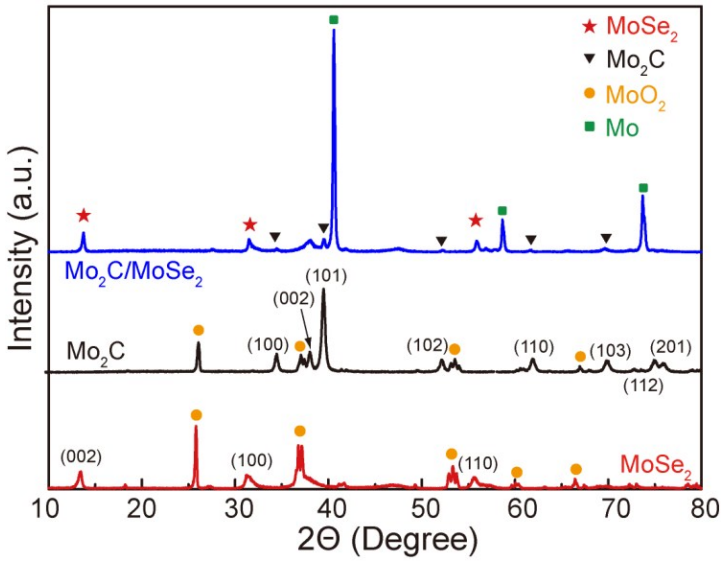

Fig. S3. X-ray diffraction patterns of $MoSe_2$, Mo_2C and $Mo_2C/MoSe_2$ materials.

Through comparison of the XRD spectra of carbonized $MoSe_2$/Mo with that of pure $MoSe_2$ and Mo_2C, it's obvious that aside from the peaks of metal Mo, the clear peaks could consist with the $MoSe_2$ and Mo_2C well, indicating that part of the $MoSe_2$ is converted into Mo_2C after the high temperature annealing in methane.

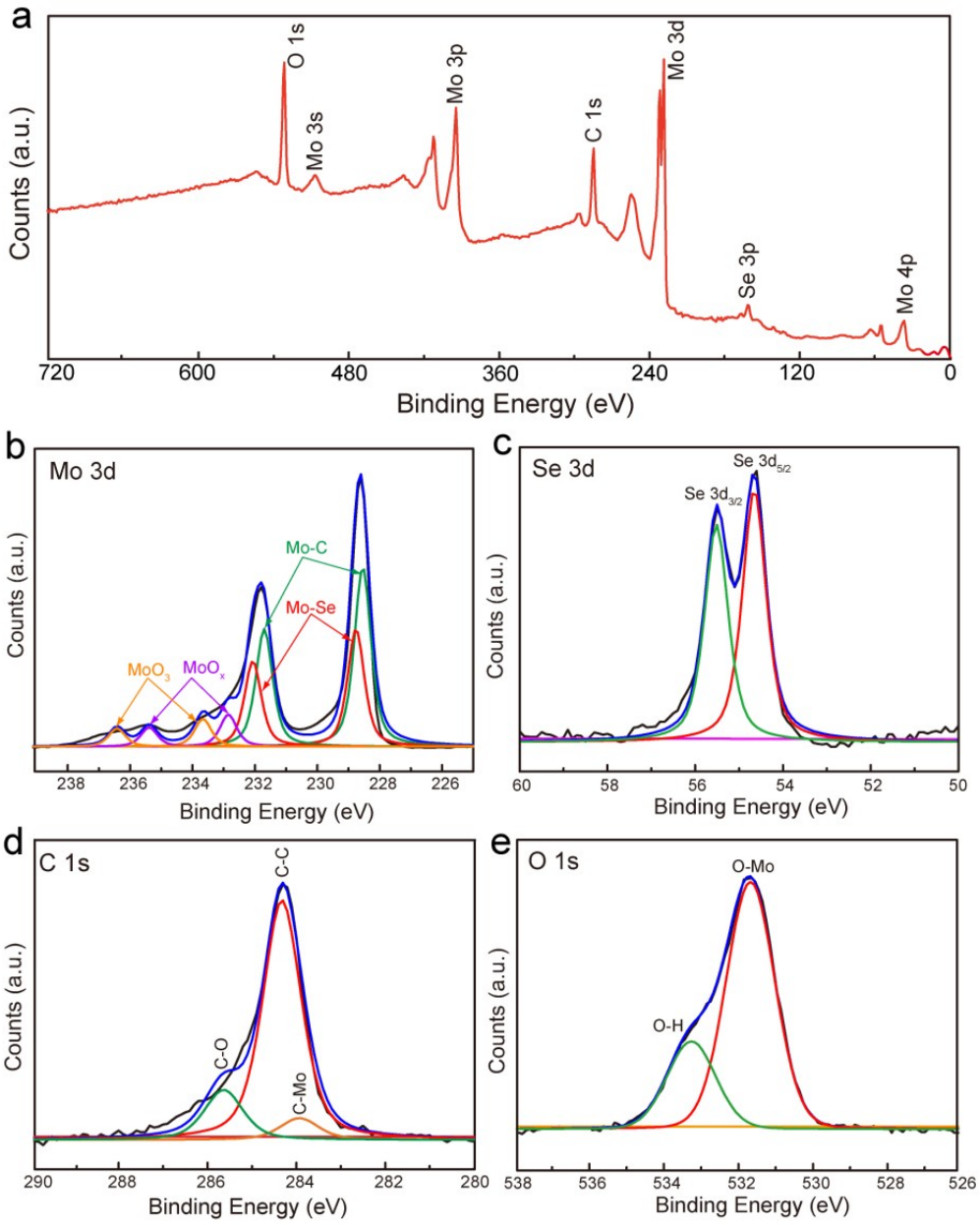

Fig. S4. (a) XPS full survey spectrum. (b) Mo 3d, (c) Se 3d, and (d) C 1s, and (e) O 1s XPS spectrum in the $Mo_2C/MoSe_2$ hybrid.

The surface electronic state and composition elements of the samples are detected by the X-ray photoelectric spectroscopy (XPS) analysis. In figure S4b, The peaks of the green line at 228.54 eV and 231.7 eV correspond to Mo^{2+} $3d_{5/2}$ and Mo^{2+} $3d_{3/2}$ of carbides, which is known to be served as active sites for HER. The peaks of the red line at the positions of 228.76 eV and 232.06 eV belong to Mo^{4+} $3d_{5/2}$ and Mo^{4+} $3d_{3/2}$. In addition, the weaker peaks in the purple and orange curves are

ascribed to Mo^{5+} and Mo^{6+}, respectively, suggesting that molybdenum oxides such as MoO_x and MoO_3 might exist in the surface of the sample. In figure S4c, the peaks appearing at 54.66 eV and 55.51 eV were attributed to Se $3d_{5/2}$ and Se $3d_{3/2}$. While the peak appeared at 533.3 eV in the XPS spectra of O 1s (Figure S4e) reveal that there are also molybdenum oxides. XPS spectra can prove the partial conversion of the $MoSe_2$ into Mo_2C.

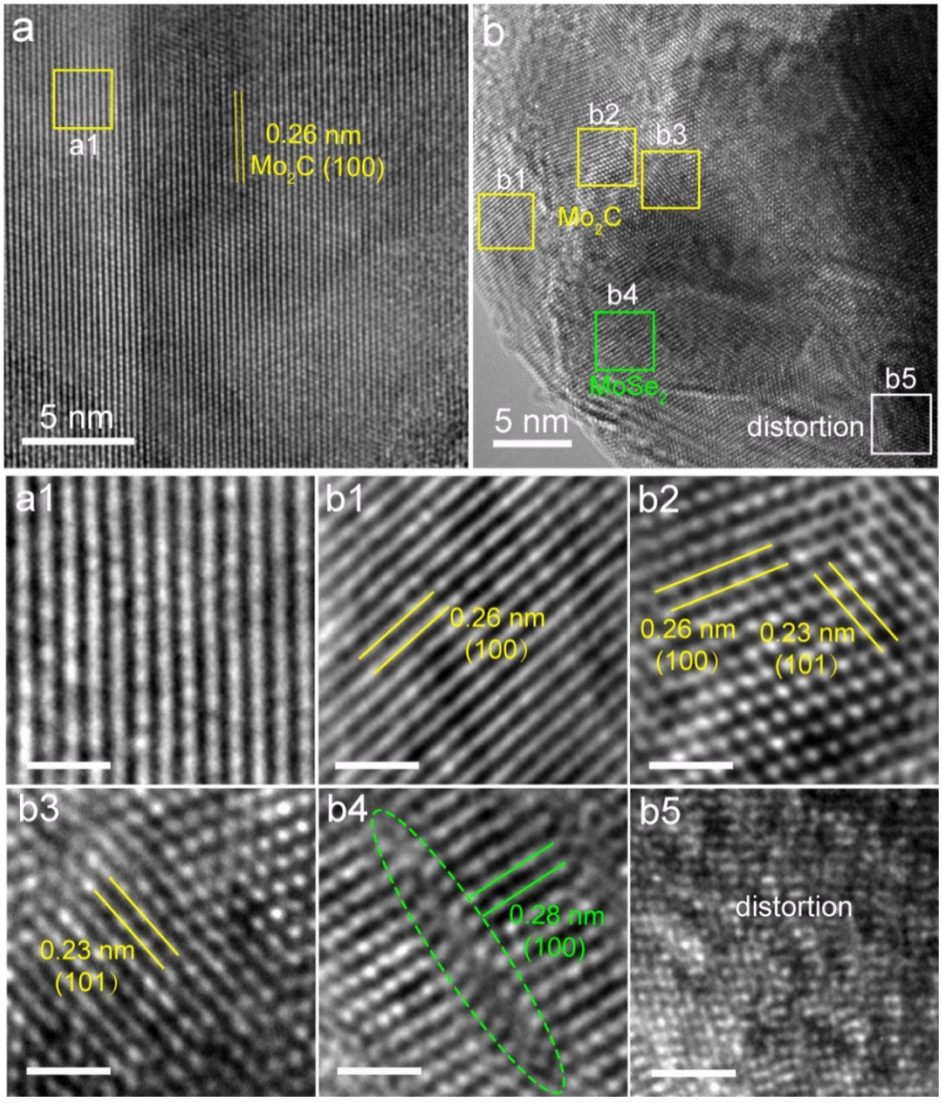

Fig. S5. HRTEM images of (a) pristine Mo_2C and (b) $Mo_2C/MoSe_2$ synthesized on the Mo foils. The scale bar in a1 and b1-b5 is 1 nm.

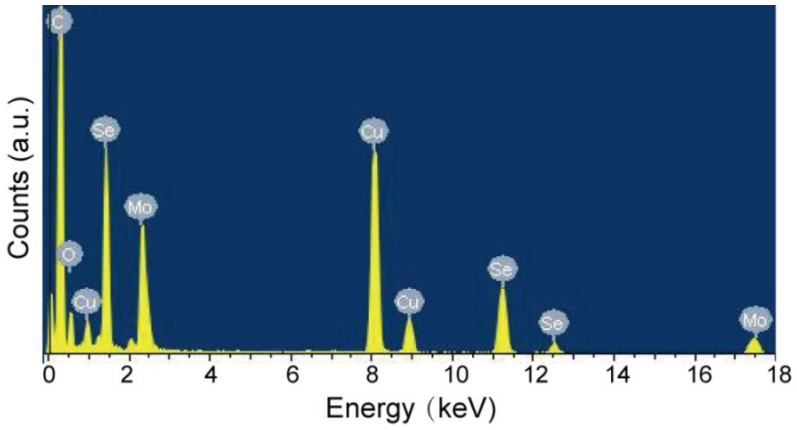

Fig. S6. EDS analysis on the chemical composition of as-prepared $Mo_2C/MoSe_2$ composite.

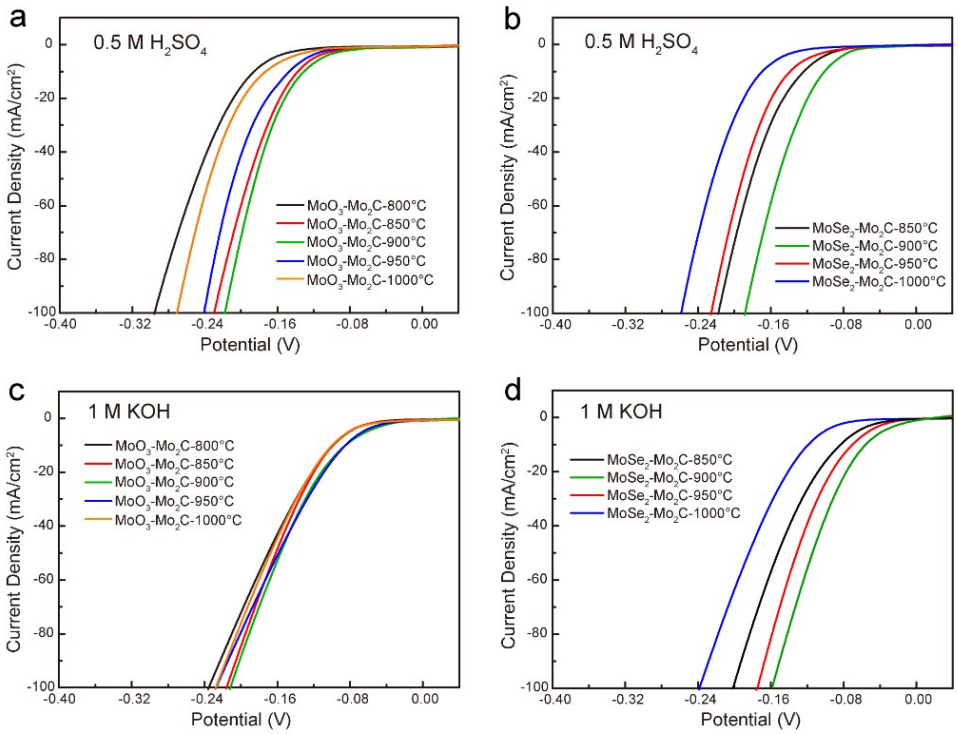

Fig. S7. The polarization curves of electrocatalysts synthesized and tested under various conditions: (a, c) Mo foils are oxidized in air at 600 °C followed by carbonization in $CH_4/H_2/Ar$ at 800, 850, 900, 950 and 1000 °C, respectively. (b, d) The sulfurization temperature of MoO_3/Mo is 600 °C, and then carbonized at 850 ~ 1000 °C. It's apparent that carbonization temperature of MoO_3 and $MoSe_2$ has effect on the HER performance of the as-prepared electrode, and both MoO_3/Mo_2C and $MoSe_2/Mo_2C$ exhibit higher HER activity in 1 M KOH than that in 0.5 M H_2SO_4.

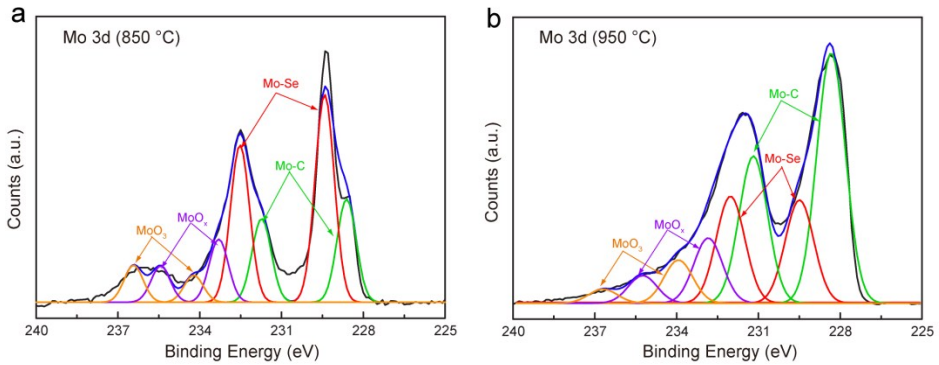

Fig. S8. XPS spectra of Mo 3d in $Mo_2C/MoSe_2$ electrocatalyst prepared at different carbonization temperature of 850 °C and 950 °C.

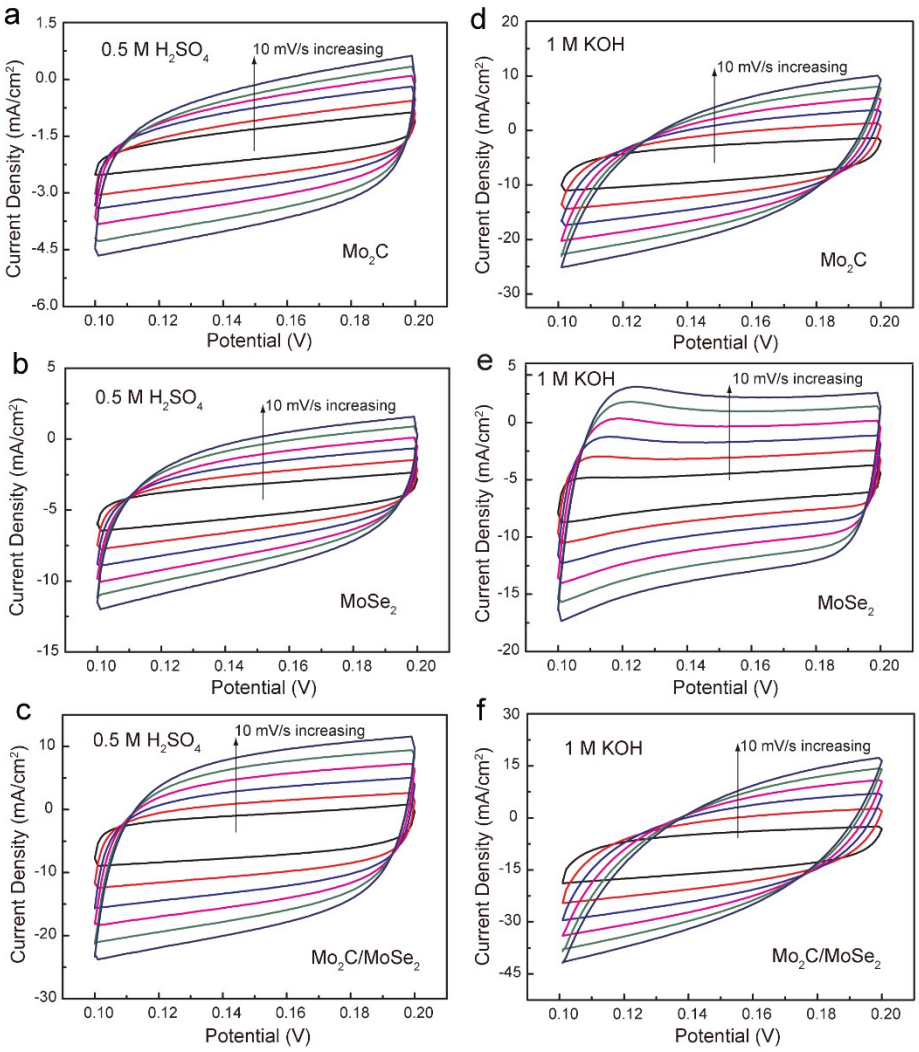

Fig. S9. Electrochemical CV tests on Mo_2C, $MoSe_2$, and $Mo_2C/MoSe_2$ with different rates from 10 to 60 mV/s in the potential range of 0.1 ~ 0.2 V in 0.5 M H_2SO_4 and 1 M KOH.

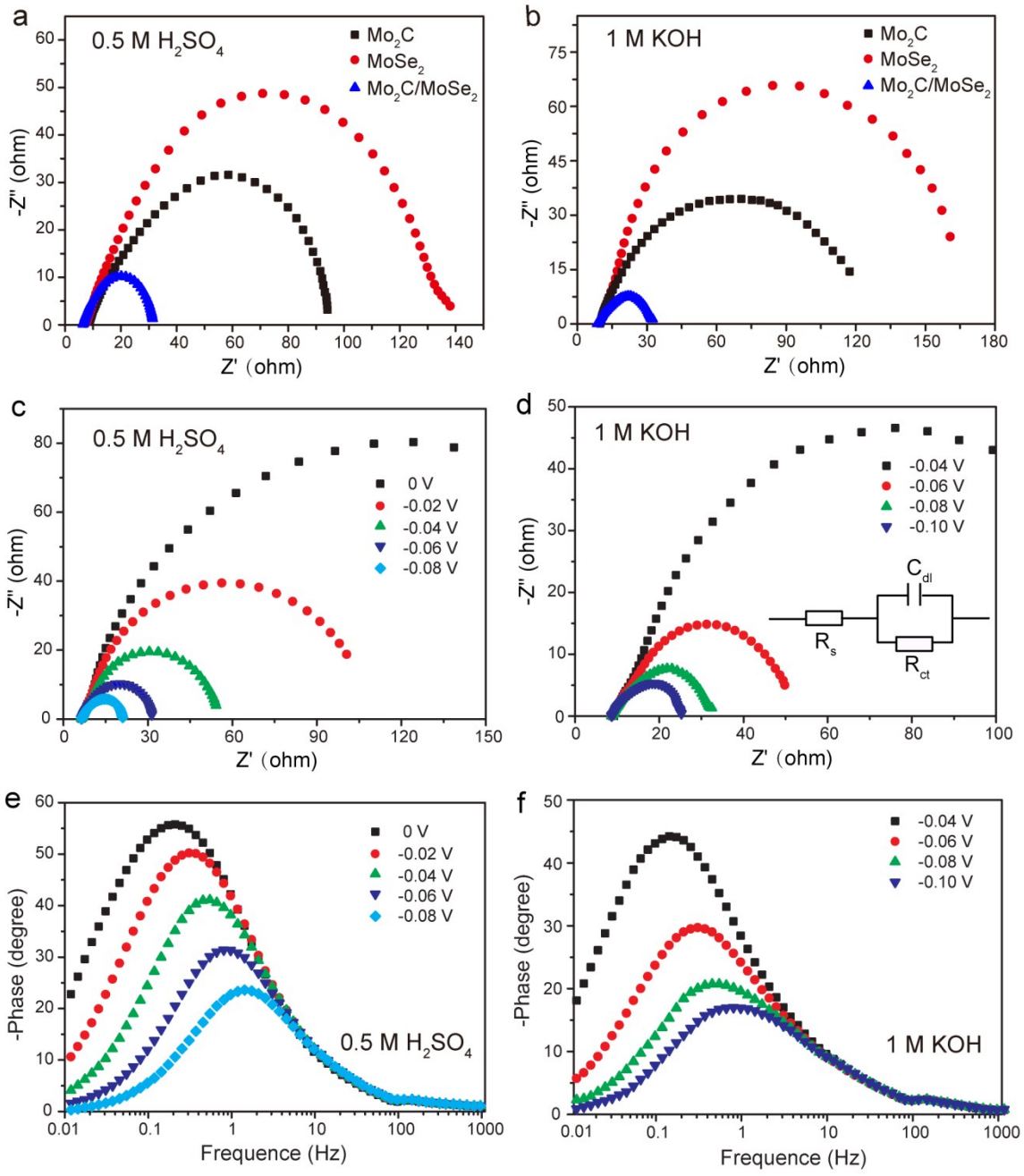

Fig. S10. (a, b) EIS Nyquist plots of Mo_2C, $MoSe_2$ and $Mo_2C/MoSe_2$ electrocatalysts collected in 0.5 M H_2SO_4 and 1 M KOH with potential of -0.06 and -0.08 V, respectively. (c, d) Nyquist plots and (e, f) Bode plots of Mo_2C-$MoSe_2$ with different applied overpotentials. Inset of figure d is the corresponding equivalent circuit diagram.

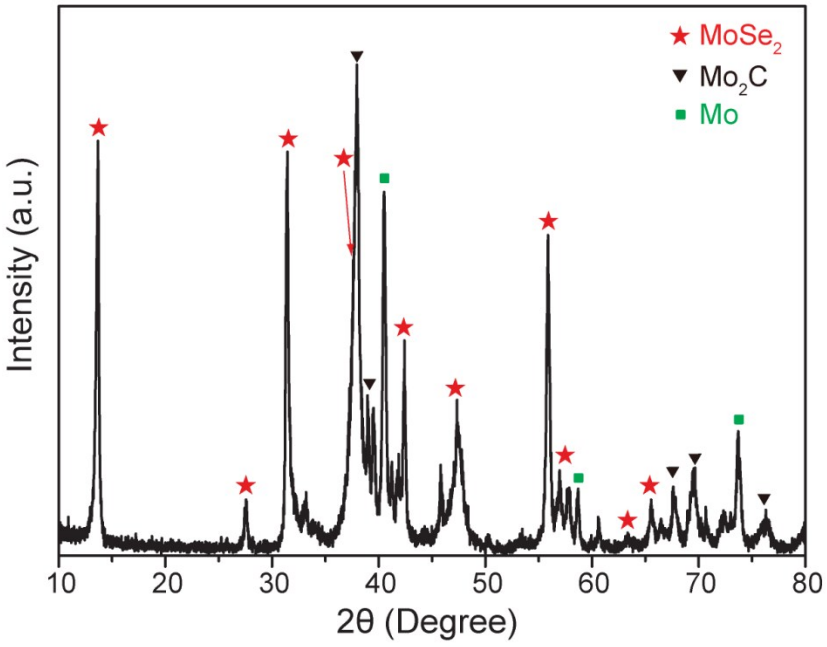

Fig. S11. XRD pattern of $Mo_2C/MoSe_2$ after stability test in in high alkaline solutions.

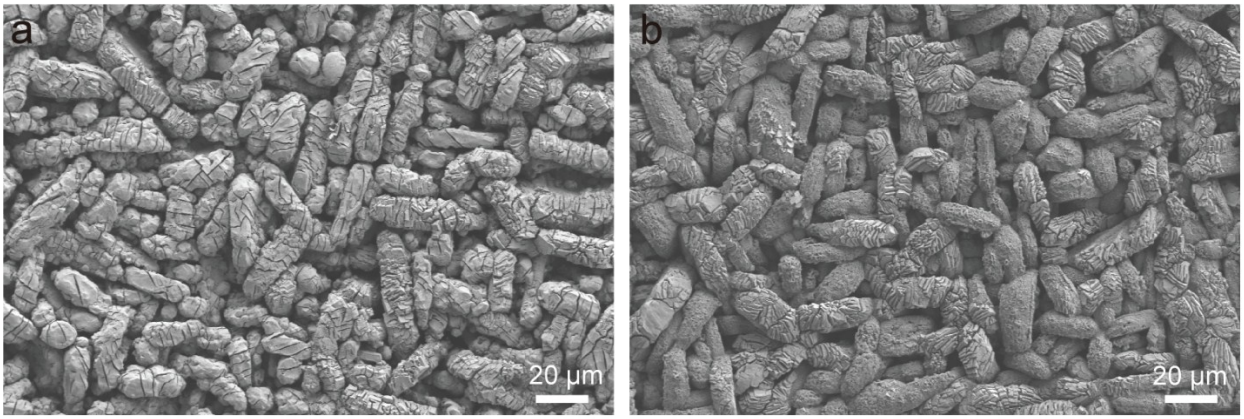

Fig S12. SEM images of $Mo_2C/MoSe_2$ after HER stability measurements in (a) 0.5 M H_2SO_4 and (b) 1 M KOH.

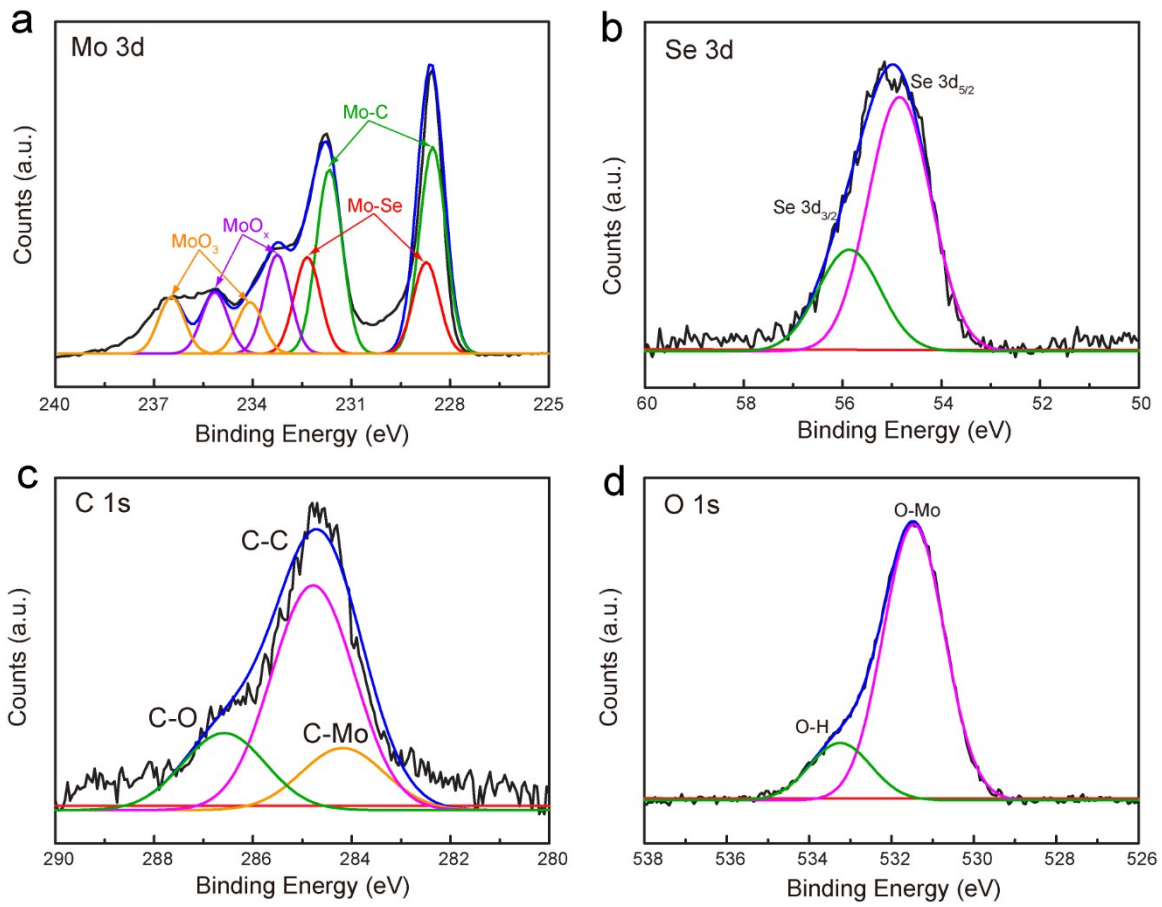

Fig. S13. XPS spectrum of (a) Mo 3d, (b) Se 3d, (c) C 1s, and (d) O 1s XPS spectrum in the $Mo_2C/MoSe_2$ hybrid after using as electrocatalysts for catalyzing HER in basic solution.

The XPS spectra of sample after HER measurements is collected to test the surface electronic state of elements. In figure S13, The peaks of the green line at 228.53 eV and 231.74 eV belong to Mo^{2+} $3d_{5/2}$ and Mo^{2+} $3d_{3/2}$ of carbides. The peaks of the red line at 228.72 eV and 232.63 eV are indexed to Mo^{4+} $3d_{5/2}$ and Mo^{4+} $3d_{3/2}$. Along with the peaks of Se 3d and C-Mo bond, we can conclude that the the Mo_2C and $MoSe_2$ are stably existing in the $Mo_2C/MoSe_2$ hybrid even after HER tests in high alkaline solutions.

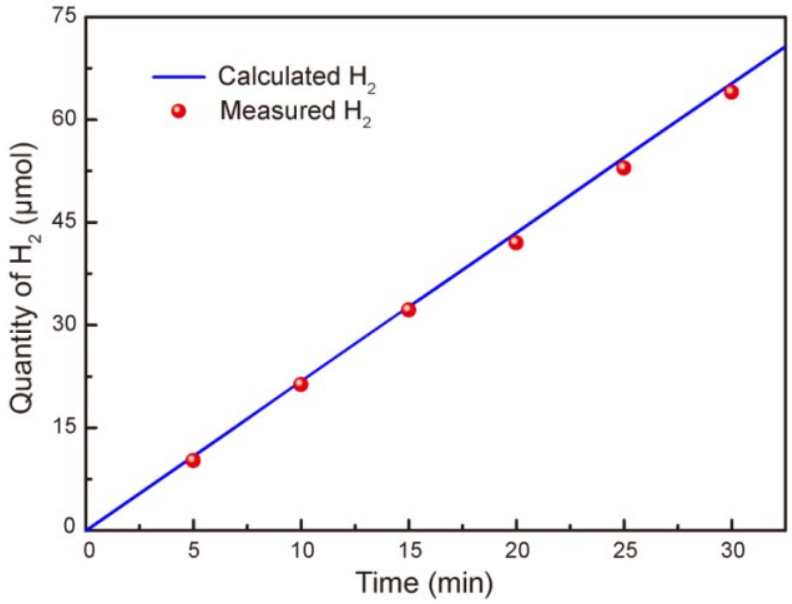

Fig. S14. Faradaic efficiency measurement by comparing the experimentally tested and theoretically calculated H_2 amounts during the HER process on the $Mo_2C/MoSe_2$ cathode at the current density of -60 mA/cm^2.

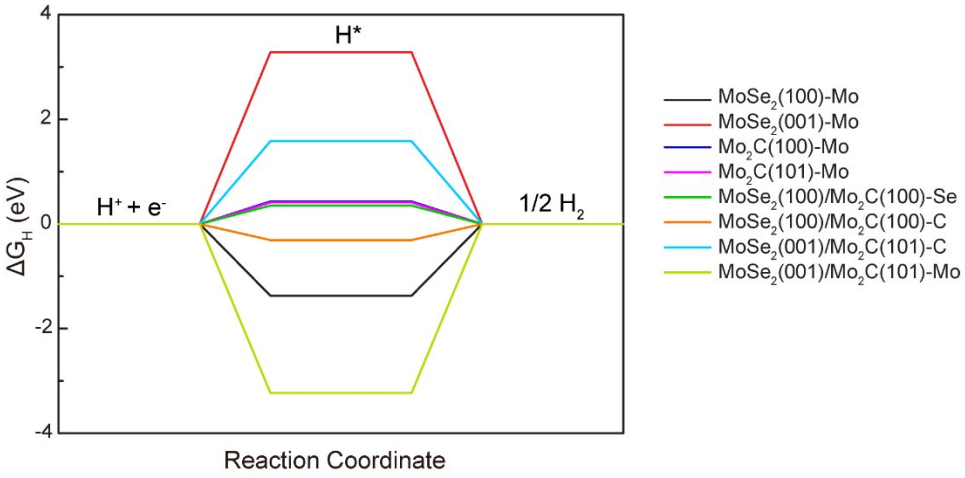

Fig. S15. Free energy diagram of the HER based on ΔG_H over the (100) and (101) planes of Mo_2C, (100) and (001) planes of $MoSe_2$, and $Mo_2C(100)/MoSe_2(100)$ and $Mo_2C(101)/MoSe_2(001)$ terrace sites. For the pristine Mo_2C and $MoSe_2$, the Mo atom is taken as active sites. While for the $Mo_2C/MoSe_2$, C, Se and Mo atom in the interface are selected as active sites, respectively.

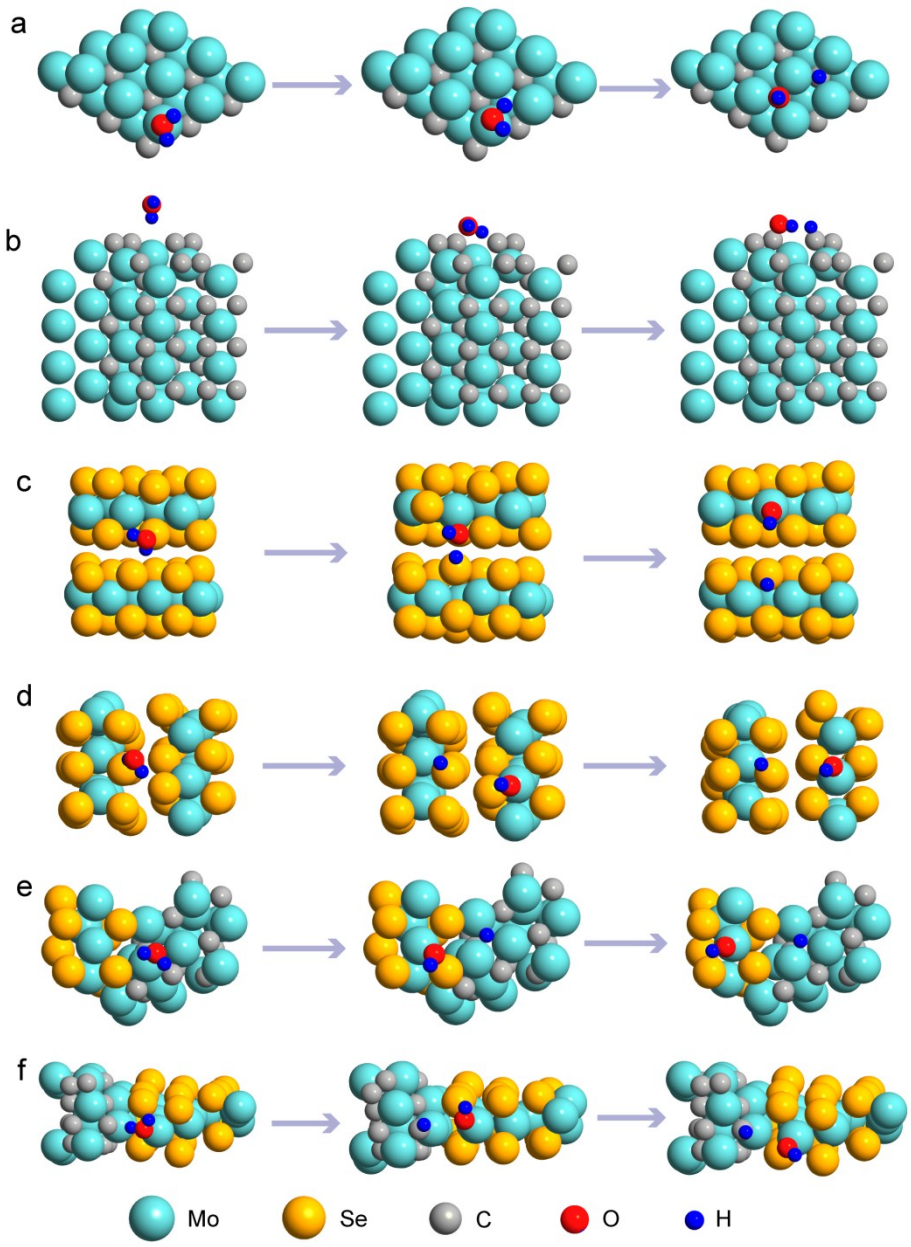

Fig. S16. Atomic structure diagram of initial, transition state and product for the water dissociation process on Mo site for (a) $Mo_2C(100)$ plane, (b) $Mo_2C(101)$ plane, (c) $MoSe_2$ (001) plane, (d) $MoSe_2$ (100) plane, (e) $MoSe_2(001)$-$Mo_2C(101)$ and (f) $MoSe_2(100)$-$Mo_2C(100)$.

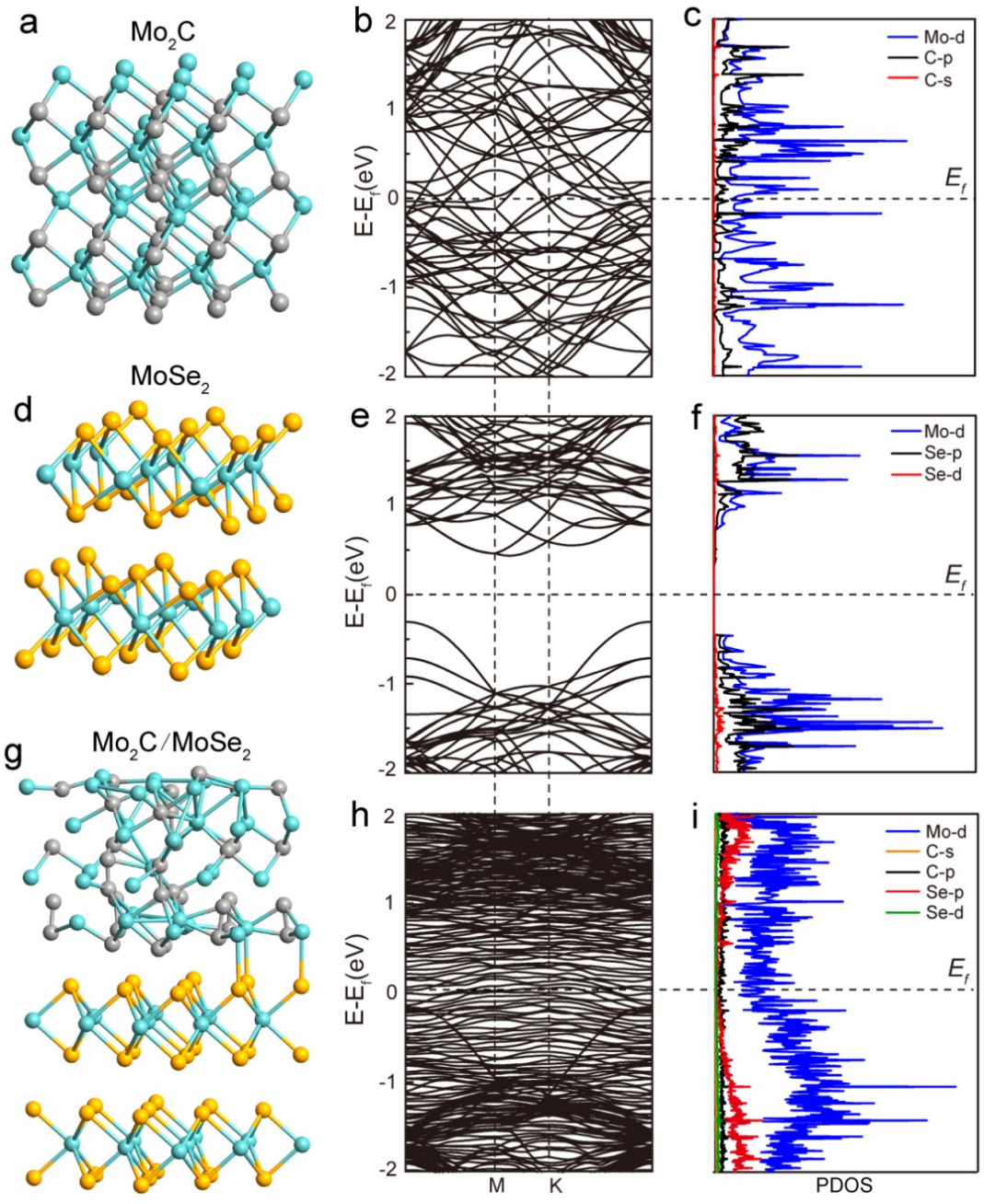

Fig. S17. The crystal structure image, band structures and PDOS of (a-c) the hexagonal $MoSe_2$, (d-f) the pristine Mo_2C and (g-i) $Mo_2C/MoSe_2$ hybrid.

Table S1. The comparison of the HER performance of Mo-based electrocatalysts tested in 0.5 M H_2SO_4 solution.

Catalyst	η_{onset} (mV) [a]	η_{10} (mV) [b]	Tafel slope (mV/dec)	Reference
$Mo_2C/MoSe_2$	**30**	**80**	**49.8**	**This work**
$MoS_2/Co_9S_8/Ni_3S_2/Ni$	~30	103	55	J. Am. Chem. Soc. 2019
Zn-MoS_2	~100	194	78	Angew. Chem. Int. Ed. 2019, 58, 1
SWCNTs/ex-$MoSe_2$:$CdCl_2$		81		Adv. Energy Mater. 2018, 8, 1801764
Mo_2N-Mo_2C/HGr	11	157	55	Adv. Mater. 2018, 30, 1704156
N@Mo_2C-3/CFP	12	56	51	Adv. Energy Mater. 2018, 8, 1800789
Mo/Mo_2C-HNS	16	89	70.72	ACS Energy Lett. 2018, 3, 341
N-doped β-Mo_2C	80	140	51.3	Appl. Catal. B: Environ. 2018, 224, 533
P-Mo_2C@C nanowires	35	89	42	Energy Environ. Sci., 2017, 10, 1262
Mo_2C@2D-NPC	~20	86	62	ACS Nano 2017, 11, 3933
N-Mo_2C NSs	48.3	99	44.5	ACS Nano 2017, 11, 12509
N@$MoPC_x$	32	108	69.4	Adv. Energy Mater. 2017, 1701601
Co-Mo_2C	40	140	39	Adv. Funct. Mater. 2016, 26, 5590
msk-MoC_x	81	146	49	ChemElectroChem 2017, 4, 2169
Mo_2C@NPC/NPRGO	0	34	33.6	Nat. Commun. 2016, 7, 11204.
MoC_x nano-octahedrons	~25	142	53	Nat. Commun. 2015, 6, 6512
nanoMoC@GS	84	124	43	J. Mater. Chem. A, 2016, 4, 6006
Mo_2C/NCF	40	144	55	ACS Nano 2016, 10, 11337
MoC-Mo_2C	38	126	43	Chem. Sci., 2016, 7, 3399
Ni-decorated Mo_2C	~60	192	98	Chem. Mater. 2016, 28, 6313
Mo_xC-Ni@NCV	~0	68	45	J. Am. Chem. Soc. 2015, 137, 15753
Mo_2C Nanotube	82	172	62	Angew. Chem. Int. Ed. 2015, 54, 15395.
Mo_2C@NC	60	124	60	Angew. Chem. Int. Ed. 2015, 27, 10902
Pure Mo_2C	80	~155	55	ACS Catal. 2015, 5, 6956
MoS_x@Mo_2C-1:8	120	~165	44	ACS Catal. 2015, 5, 6956
nw-W4MoC	~80	~30	52	Adv. Funct. Mater. 2015, 25, 1520
Mo_2C-G	~0	150	57	Chem. Commun. 2015, 51, 8323
Mo_2C/CC	30	140	124	J. Mater. Chem. A, 2015, 3, 16320
NiMo_2C/NF	21	150	36.8	J. Mater. Chem. A, 2015, 3, 1863
Mo_2C/C	6	78	41	Angew. Chem. Int. Ed. 2015, 54,14723
Mo_2C nanowires	70	130	54	Energy Environ. Sci. 2014, 7, 387
Mo_2C/CNT-GR	62	130	58	ACS Nano. 2014, 5, 5164

[a] η_{onset} means the onset potential (vs RHE) of the electrocatalysts. [b] η_{10} refer to the overpotentials vs RHE at cathodic current densities of 10 mA/cm^2.

Table S2. The comparison of the HER activity of Mo-based electrocatalysts measured in 1 M KOH electrolyte.

Catalyst	η_{onset} (mV)[a]	η_{10} (mV)[b]	Tafel slope (mV/dec)	Reference
$Mo_2C/MoSe_2$	**~0**	**51**	**47.6**	**This work**
NiO@1T-MoS_2	~0	46	52	Nat. Commun. 2019, 10, 982
C–MoS_2	~0	45	46	Nat. Commun. 2019, 10, 1217
$MoS_2/Co_9S_8/Ni_3S_2$/Ni	~20	113	85	J. Am. Chem. Soc. 2019
Ir-MoS_2	~0	44	32	ACS Energy Lett. 2019, 4, 368
SWCNTs/ex-$MoSe_2$:$CdCl_2$		64		Adv. Energy Mater. 2018, 8, 1801764
Ni/Mo_2C-NCNFs	29	143	57.8	Adv. Energy Mater. 2019, 9, 1803185
Mo_2N-Mo_2C/HGr	18	154	58	Adv. Mater. 2018, 30, 1704156
N@Mo_2C-3/CFP	~40	66	49	Adv. Energy Mater. 2018, 8, 1800789
Mo/Mo_2C-HNS	10	79	62.9	ACS Energy Lett. 2018, 3, 341
N-doped β-Mo_2C nanobelts	52	110	49.7	Appl. Catal. B: Environ. 2018, 224, 533
B,N: Mo_2C@BCN	~40	100	62	ACS Catal. 2018, 8, 8296
Mo_2C@2D-NPC	~0	45	46	ACS Nano 2017, 11, 3933
N-Mo_2C NSs	69	140	65	ACS Nano 2017, 11, 12509
N@$MoPC_x$	45	139	96.6	Adv. Energy Mater. 2017, 1701601
Co-Mo_2C	25	118	44	Adv. Funct. Mater. 2016, 26, 5590
msk-MoC_x	50	101	44	ChemElectroChem 2017, 4, 2169
MoC_x nano-octahedrons	~80	151	59	Nat. Commun. 2015, 6, 6512
nanoMoC@GS	42	77	50	J. Mater. Chem. A, 2016, 4, 6006
Mo_2C/NCF	10	100	65	ACS Nano 2016, 10, 11337
MoC-Mo_2C heteronanowires	33	120	42	Chem. Sci., 2016, 7, 3399
Ni-decorated Mo_2C	~30	123	83	Chem. Mater. 2016, 28, 6313
Mo_xC-Ni@NCV	~0	126	93	J. Am. Chem. Soc. 2015, 137, 15753
Mo_2C Nanotube	37	112	55	Angew. Chem. Int. Ed. 2015, 54, 15395.
Mo_2C@NC	10	60		Angew. Chem. Int. Ed. 2015, 27, 10902

[a] η_{onset} means the onset potential (vs RHE) of the electrocatalysts. [b] η_{10} refer to the overpotentials vs RHE required to afford the cathodic current densities of 10 mA/cm^2.

References

S1 J. X. Zhang, H. Cheng, Y. Z. Chen, A. Uddin, S. Yuan, S. J. Geng, and S. Zhang, *Surface &Coatings Technology,* 2005, **198**, 68-73.

S2 P. A. Gabrys, S. E. Seo, M. X. Wang, E. Oh, R. J. Macfarlane, and C. A. Mirkin, *Nano Lett.,* 2018, **18**, 579-585.

S3 http://www.quantumwise.com/ for QuantumWise Atomistix ToolKit (ATK).

S4 N. Helbig, J. I. Fuks, M. Casula, M. J. Verstraete, M. A. L. Marques, I. V. Tokatly, and A. Rubio, *Phys. Rev. A*, 2011, **83**, 032503.

S5 H. J. Monkhorst and J. D. Pack, *Phys. Rev. B*, 1976, **13**, 5188-5192.

S6 P. Pulay, *Chem. Phys. Lett.*, 1980, **73**, 393-398.

S7 https://wiki.fysik.dtu.dk/ase/ase/optimize.html.